

LETTER TO THE EDITOR

The HARPS search for southern extra-solar planets**XLII. A system of Earth-mass planets around the nearby M dwarf YZ Cet ^{★,★★}**

N. Astudillo-Defru¹, R. F. Díaz^{2,3}, X. Bonfils⁴, J.M. Almenara¹, J.-B. Delisle¹, F. Bouchy¹, X. Delfosse⁴, T. Forveille⁴, C. Lovis¹, M. Mayor¹, F. Murgas⁷, F. Pepe¹, N. C. Santos^{5,6}, D. Ségransan¹, S. Udry¹, A. Wünsche⁴

¹ Observatoire de Genève, Université de Genève, 51 ch. des Maillettes, 1290 Sauverny, Switzerland² Universidad de Buenos Aires, Facultad de Ciencias Exactas y Naturales, Buenos Aires, Argentina.³ CONICET - Universidad de Buenos Aires, Instituto de Astronomía y Física del Espacio (IAFE), Buenos Aires, Argentina.⁴ Univ. Grenoble Alpes, CNRS, IPAG, F-38000 Grenoble, France⁵ Instituto de Astrofísica e Ciências do Espaço, Universidade do Porto, CAUP, Rua das Estrelas, PT4150-762 Porto, Portugal⁶ Departamento de Física e Astronomia, Faculdade de Ciências, Universidade do Porto, Portugal⁷ Instituto de Astrofísica de Canarias, Vía Láctea s/n, E-38205 La Laguna, Tenerife, Spain**ABSTRACT**

Exoplanet surveys have shown that systems with multiple low-mass planets on compact orbits are common. Except for few cases, however, the masses of these planets are generally unknown. At the very end of the main sequence, host stars have the lowest mass and hence offer the largest reflect motion for a given planet. In that context, we monitored the low-mass ($0.13M_{\odot}$) M dwarf YZ Cet (GJ 54.1, HIP 5643) intensively and obtained both radial velocities and stellar-activity indicators derived from both spectroscopy and photometry. We find strong evidence that it is orbited by at least three planets in compact orbits ($P_{Orb}=1.97, 3.06, 4.66$ days), with the inner two near a 2:3 mean-motion resonance. The minimum masses are comparable to that of Earth ($M_{\sin i}=0.75\pm0.13, 0.98\pm0.14$, and $1.14\pm0.17 M_{\oplus}$) and also the lowest masses measured by radial velocity so far. We note the possibility for an even lower-mass, fourth planet with $M_{\sin i}=0.472\pm0.096 M_{\oplus}$ at $P_{Orb}=1.04$ days. An n-body dynamical model is used to put further constraints on the system parameters. At 3.6 parsecs, YZ Cet is the nearest multi-planet system detected to date.

Key words. stars: individual: YZ Cet – stars: planetary systems – stars: late-type – technique: radial velocities

1. Introduction

In about twenty years we have learned about the vast diversity in the architecture of planetary systems (e.g. Mayor et al. 2014; Fabrycky et al. 2014). For stars of different spectral types we have discovered a large variety of planets in mass and size, constraining our understanding of planetary formation processes.

M dwarfs are about 70% of the stellar population of the Galaxy and constitute the lower tail of the main sequence in the Hertzsprung–Russell diagram. The detection of planets orbiting these stars is therefore important to constrain the population of planets and the formation processes in the less-massive protoplanetary disks (Gaidos 2017). Additionally, low-mass and small-size M dwarfs have advantages when searching for the lowest-mass and smallest-size planets: the radial velocity (RV) amplitude and transit depth scales with $M_{\star}^{-2/3}$ and R_{\star}^{-2} , respectively.

It is known that M dwarfs have a high occurrence of super-Earths as shown from high precision radial velocity ($f\sim0.88$ for $P<100$ days and $M_{\sin i}=1\text{--}10 M_{\oplus}$, Bonfils et al. 2013) and transits surveys (Dressing & Charbonneau 2015, $f\sim2.5$ for $P<200$

days and $R=1\text{--}4 R_{\oplus}$). Now thanks to the most precise velocimeters combined to the high amount of collected data we are starting to census planets with minimum masses closer to the Earth mass as, e.g. GJ 273 c (Astudillo-Defru et al. 2017b), Prox Cen b (Anglada-Escudé et al. 2016) or GJ 628 b (Wright et al. 2016).

The detection of multi-planetary systems sheds light on the theories of model formation and evolution. Statistical studies have shown that planet pairs near or in mean-resonances are slightly favored (e.g. Fabrycky et al. 2014). In the understanding of this scenario a low uncertainty in the measured mass is important, however, the majority of the systems has been detected by transits, were uncertainties are generally too large for a reliable physical characterization of the planets (e.g. Kepler-42, Trappist-1, Muirhead et al. 2012; Gillon et al. 2017, resp.).

In this paper we present a new nearby system (3.6 pc) of a very-low-mass star orbited by at least three Earth-mass planets in compact orbits, with the possibility of a fourth sub-Earth-mass companion.

2. Stellar properties and Observations**2.1. Stellar properties**

The properties of the mid-M dwarf YZ Cet are given in Table 1. The table lists, the visual and near infrared apparent magnitudes, the parallax and proper motions, basic physical parameters, the activity level and age. These values come from the literature detailed in the table caption.

[★] Based on observations made with the HARPS instrument on the ESO 3.6 m telescope under the program IDs 180.C-0886(A), 183.C-0437(A), and 191.C-0873(A) at Cerro La Silla (Chile).

^{★★} Radial velocity data (Tables XXX) are only available at the CDS via anonymous ftp to cdsarc.u-strasbg.fr (130.79.128.5) or via <http://cdsarc.u-strasbg.fr/viz-bin/qcat?J/A+A/XXX/XXX>

Table 1. Stellar properties.

R.A. ¹	[J2000]	01 ^h 12 ^m 30.5 ^s
Decl. ¹	[J2000]	-16°59'56"
Spectral type ¹		M4.5
V ¹		12.074
J ²		7.258±0.020
K ²		6.420±0.017
π^3	[mas]	271.01±8.36
μ_a^3	[mas/yr]	1208.53±5.57
μ_δ^3	[mas/yr]	640.73±3.71
dv_r/dt	[m/s/yr]	0.159±0.006
M ¹	[M _⊙]	0.130±0.013
R ¹	[R _⊙]	0.168±0.009
T _{eff} ¹	[K]	3056±60
[Fe/H] ¹		-0.26±0.08
log(R' _{HK}) ⁴		-4.71±0.21
Age ⁵	[Gyr]	5.0±1.0

¹ Mann et al. (2015, 2016); ² Cutri et al. (2003); ³ van Leeuwen (2007); ⁴ Astudillo-Defru et al. (2017a); ⁵ Engle & Guinan (2011, assuming P_{Rot} = 83±15 d)

2.2. HARPS radial velocities

We observed YZ Cet from December, 2003 to October, 2016 with the HARPS spectrograph installed at the ESO 3.6m telescope, in Chile (Mayor et al. 2003). A total of 211 spectra were acquired with an exposure time of 900 s and fast read-out mode, corresponding to a typical signal-to-noise ratio per spectra of 19 at 550 nm. Data were recorded without simultaneous wavelength reference to keep stellar low-flux zones free of lamp contamination. The HARPS vacuum vessel was opened on May, 2015 to upgrade the fiber link (Lo Curto et al. 2015, in what follows a “+” superscript indicates data acquired after the upgrade). This modifies the line-spread function and may affect the spectral analysis. Consequently, for some of our analyses we independently analyze the pre- and post-fiber upgrade data sets.

2.3. ASAS photometry

This work uses data from the All Sky Automated Survey (ASAS) (Pojmanski 1997). The ASAS project constantly monitors a large area of the sky (9° × 9°) to look for photometric variability in V- and I-band. The ASAS photometric accuracy is 0.01–0.02 mag for a 13th magnitude star, being enough to detect spots crossing the stellar disc due to rotation.

The used ASAS data of YZ Cet consists in 459 photometric measurements acquired from November, 2000 to November 2009. Unfortunately ASAS and HARPS data do not overlap in time, which is desired in the understanding of RV variability non produced by planets. We used the two pixels wide aperture (MAG_0) as suggested by ASAS for a 12.07 Vmag star.

3. Analysis

3.1. Periodogram+Keplerian

We computed the generalized Lomb-Scargle periodogram (Zechmeister & Kürster 2009) of the RVs and residues from progressively subtracting a Keplerian fit accounting for the strongest peak in the periodogram (Fig. 1). We adjusted up to four Keplerian curves plus a velocity offset between the data obtained before and after the HARPS fibre upgrade (BJD=2457172, Lo

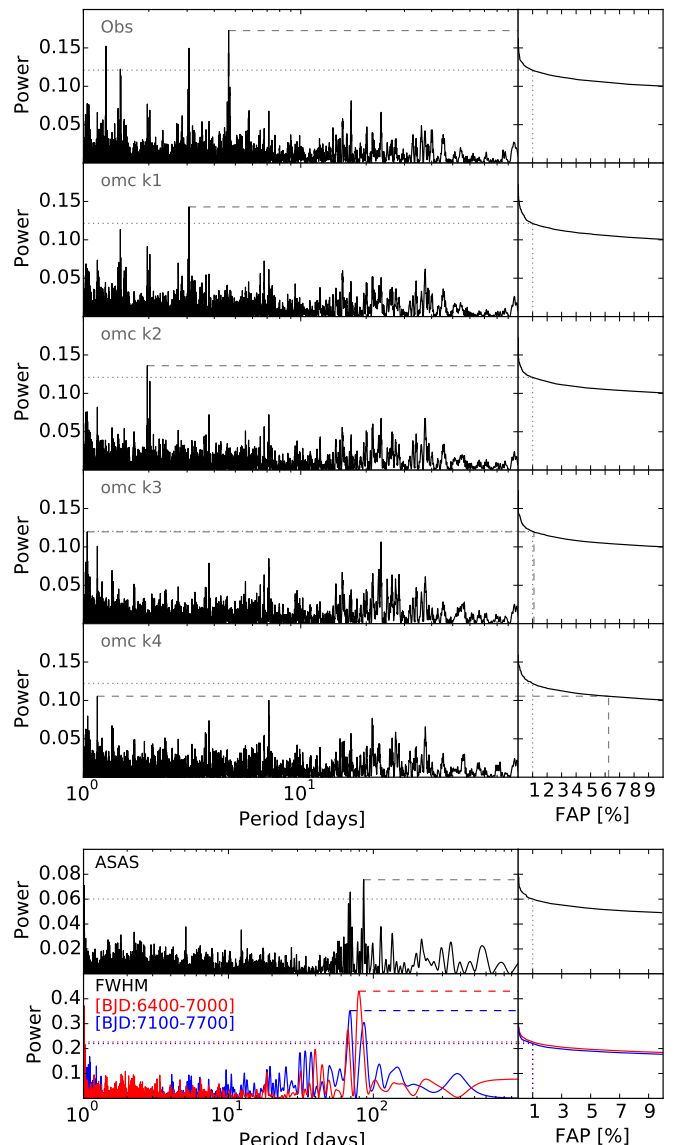


Fig. 1. Periodogram analysis of the RV (top panel), and the ASAS photometry and FWHM_{CCF} (bottom panel). Dashed lines highlight the strongest peaks, dotted lines represent the 1% FAP threshold. Three RV signals are under 1%FAP while a fourth is just above this level of confidence. Final RV residual (omc k4) does not show any significant periodicity. The photometry and FWHM_{CCF} show a ~83-days periodicity linked to the stellar rotation. Pre- (red) and post- (blue) fibers upgrade data are separately analyzed

Curto et al. 2015). The top panel in Figure 1 shows three clear periodic RV signals at 4.7, 3.1, and 2.0 days, with a false-alarm-probability (FAP) <1/10,000. A fourth less clear signal is seen with a 1 day periodicity and a 1.1% FAP. The Bayesian Information Criterion (BIC) for a constant model is 857.83 and for a model of one, two, three, and four Keplerian the BIC results in 463.57, 420.21, 392.62, and 376.10, respectively. On the one hand the BIC favours the model consisting in four Keplerian curves, but on the other hand the FAP of the fourth signal is above the 1% FAP threshold. We prefer to stay in the conservative side and consider the fourth signal as tentative. A more rigorous Bayesian model comparison and/or additional data are needed to elucidate the reliability on the 1-day RV signature.

3.2. Stellar activity

YZ Cet is an active star with $\log(R'_{HK}) = -4.705 \pm 0.208$. Such a R'_{HK} level translates into a rotation period of 27 ± 9 days (Astudillo-Defru et al. 2017a). However, there are clues that flaring stars, like Proxima Centauri, do not follow the $\log(R'_{HK}) - P_{Rot}$ relationship. This is the case for YZ Cet, where several flares are identified in spectra through Ca II HK, Na D, He I D3, and $\text{H}\alpha\beta\gamma\delta$. These chromospheric activity indicators do not show evidence of the stellar rotation.

Contrary to the chromospheric activity indicators, the V-band photometry and the FWHM show evidence of the rotation period of YZ Cet (~ 83 days, Fig. 1). Inversely, none of the periodicities detected in the radial velocity time series appear in the photometry or FWHM data.

3.3. Three Keplerian+Gaussian Process

As the star rotates, quasi-periodic signals may be introduced in RV due to evolving active regions. These signals are often very complex, and therefore a physical model is usually hard to produce or has the strong disadvantage of being computationally expensive. Gaussian processes regression (GP) has become a widely-used non-parametric method to model this variability without the necessity to specify a model (Rasmussen & Williams 2006; Haywood et al. 2014; Rajpaul et al. 2015; Faria et al. 2016), although it may be prone to induce false positives if care is not taken (Dumusque et al. 2017).

A GP with a quasi-periodic covariance function is added to the three-Keplerian model. The GP hyperparameters are sampled together with the model parameters. We set a normal prior on the recurrence time scale, \mathcal{P} (see Appendix A), centred at 83 days and with a width of 15 days, in agreement to the measured stellar rotation rate (see Sect. 3.2). A detailed description of the model and the choice of priors is found in Appendix A.

The 23-dimensional parameter space of our model was explored with the MCMC algorithm described in Goodman & Weare (2010) and implemented by Foreman-Mackey et al. (2013), where 100 walkers were used. The algorithm was started at a random point in the prior and was allowed to evolve until no further variation of the mean posterior density across the walkers was seen. Then, the algorithm was run for a further 100,000 steps used for the inference process. We retained only those walkers that explored the main period peak for each planet (Fig 1), whose samples were used to initialise a new 70,000-step MCMC run using 300 walkers. The final inference is done on 2.1×10^7 posterior samples, out of which over 21,000 are independent (see Appendix B for details). Results are reported in Table B.

4. Results

4.1. A compact system near the 3:2 resonances

Both the periodogram and activity analysis (Sect. 3.1, 3.2) give strong evidence that the very-low-mass-star YZ Cet is orbited by at least three planets in a compact architecture. From the Keplerian modelling combined with the Gaussian Processes we obtain orbital periods of 4.66, 3.06, and 1.97 days, that is, orbits close to the 3:2 mean-motion resonances. Considering the stellar mass of $0.13M_{\odot}$, the measured semi-amplitude translates into terrestrial-mass planets with minimum masses of 1.14, 0.98, and 0.75 Earth-masses, respectively. Table 2 gives the basic parameters of the system. Figure 2 shows the RV folded to each period.

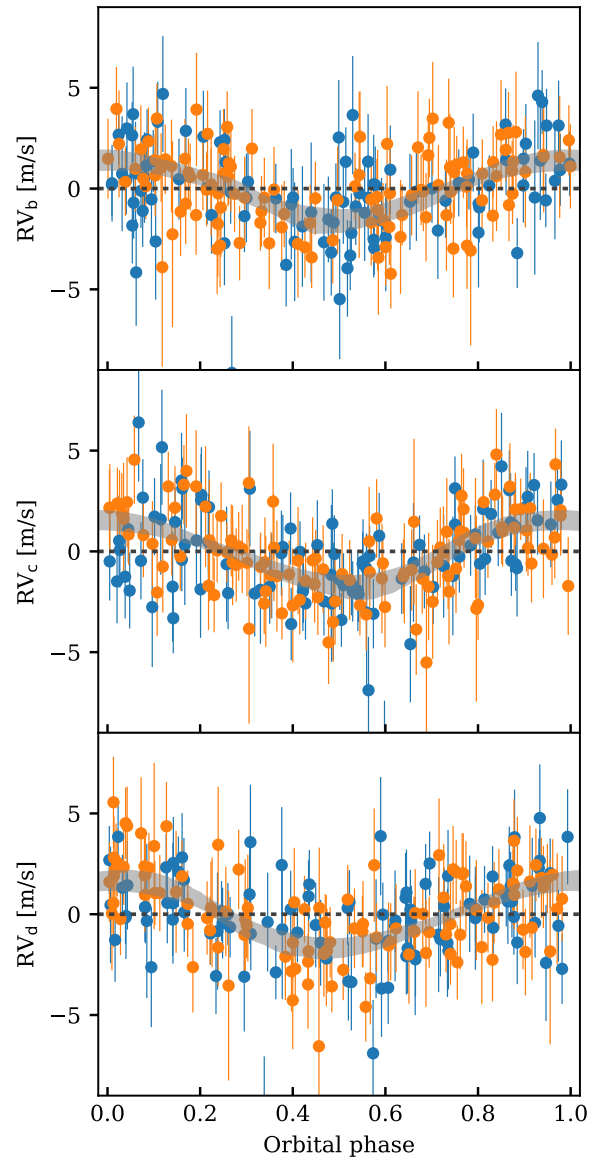


Fig. 2. Radial velocities folded to each maximum-a-posteriori orbital period (planets b, c, and d from top to bottom, respectively). Gray shaded regions extend between the 5th and 95th percentile of the model at each orbital phase, computed over 10,000 samples of the posterior. Orange and blue circles depict data before and after the HARPS fibre upgrade, respectively.

4.2. Dynamical modelling

We show in Figure 3 a stability analysis focused on Planet c where all orbital parameters are fixed to the maximum-a-posteriori (MAP) solution, and we vary only the semi-major axis and the eccentricity. For each set of initial conditions we integrate the system for 1 kyr using GENGA (Grimm & Stadel 2014), and compute the NAFF stability indicator (Laskar 1990, 1993; Correia et al. 2005). There we see that the MAP solution is stable and outside both 3:2 mean-motion resonances. We also see that $e_c \lesssim 0.1$ is needed for the system to remain stable.

Additionally, we use the n-body code REBOUND (Rein & Liu 2012) with the WHFast integrator (Rein & Tamayo 2015) to obtain the RV of the bodies in time that we compare them with the HARPS data. A stability criteria is imposed based on an additional n-body integration of 1 kyr in the future. The change

Table 2. Basic orbital parameters of the planets. All parameters can be found in Table B.

	YZ Cet b	YZ Cet c	YZ Cet d	
$M \sin i$	[M_{Earth}]	0.75 ± 0.13	0.98 ± 0.14	1.14 ± 0.17
P	[days]	1.96876	3.06008	4.65627
	[days]	± 0.00021	± 0.00022	± 0.00042
e		0.00 ± 0.12	0.04 ± 0.11	0.129 ± 0.096
a	[au]	0.01557	0.02090	0.02764
	[au]	± 0.00052	± 0.00070	± 0.00093

in the period of a planet in 1 kyr ($\Delta P_{1 \text{ kyr}}$) is extrapolated to 5 Gyr (the estimated age of the system) assuming $\Delta P_{5 \text{ Gyr}} \sim \Delta P_{1 \text{ kyr}} \sqrt{5 \text{ Gyr}/1 \text{ kyr}}$. The model is rejected if $\Delta P_{5 \text{ Gyr}}$ is bigger than the measured orbital period, which is a conservative criteria rejecting unstable configurations. We use a normal distribution as prior for the stellar mass (Table 1) and uniform priors for the rest of parameters. The emcee algorithm (Goodman & Weare 2010; Foreman-Mackey et al. 2013) is used to sample the posterior distribution of the parameters. We estimate the planet masses without the degeneracy with the orbital inclination relative to the line of sight by modelling the gravitational interaction between the three well known planets in the system. From this preliminary analysis, until the fourth signal is confirmed (rejected), we obtain: $M_b = 1.30^{+1.0}_{-0.56} M_{\oplus}$, $M_c = 2.1^{+1.5}_{-1.0} M_{\oplus}$, $M_d = 1.74^{+1.3}_{-0.51} M_{\oplus}$ (median and 68.3% credible interval), thanks to the constrain on the inclination: 95% HDI $i_b[10, 172]^\circ$, $i_c[6, 174]^\circ$, $i_d[28, 174]^\circ$. Also more tight constrains are obtained for the measured planet's eccentricities $e_b < 0.39$, $e_c < 0.15$, $e_d < 0.17$ at 95%.

5. Conclusions

We present the discovery of three terrestrial-mass planets orbiting the very-low-mass star YZ Cet. The best fit (three Keplerian+GP) to our 13-years of HARPS data results in compact orbits close to the 3:2 mean-motion resonance with orbital periods of 1.97, 3.06, and 4.66 days. The measured minimum masses are 0.75, 0.98, and 1.14 Earth-masses, respectively, with a typical uncertainty of 16%. A fourth planet with a minimum mass of 0.42 ± 0.11 and orbital period of 1.0419 days may be present in the system (1.1%FAP). To date, these are the smallest minimum masses measured by radial velocity.

From a dynamical analysis we infer the upper limits of the planetary masses, resulting in masses below 3 Earth-masses. It is probable that these have radii up to $1.5 R_{\oplus}$ (Fulton et al. 2017) with a rocky bulk composition. The planets orbit outside the habitable zone of YZ Cet, with equilibrium temperatures ranging 347–491 K, 299–423 K, and 260–368 K, for planets b, c, and d, respectively.

The the system is at only 3.6 pc, making it very attractive for further characterization, specially if any of the planets is caught transiting its host star, which to date is not the case.

Acknowledgements. NAD and FP acknowledges the support of the Swiss National Science Foundation project 166227. NCS acknowledges support from Fundação para a Ciência e a Tecnologia (FCT) through national funds and from FEDER through COMPETE2020 by the grants UID/FIS/04434/2013 & POCI-01-0145-FEDER-007672 and PTDC/FIS-AST/1526/2014 & POCI-01-0145-FEDER-016886. NCS also acknowledges the support from FCT through Investigador FCT contract IF/00169/2012/CP0150/CT0002. We made use of the REBOUND code which can be downloaded at <http://github.com/hannorein/rebound>. These simulations have been run on the *Regor* cluster kindly provided by the Observatoire de Genève.

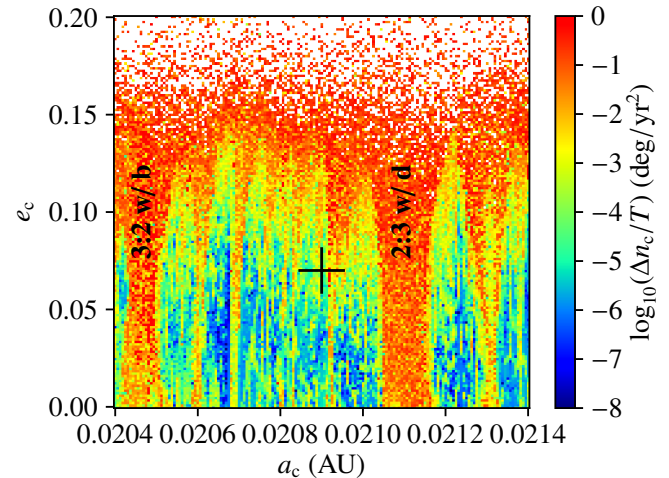


Fig. 3. Stability analysis around the MAP solution (marked with a black cross, see Table B). Blue points correspond to stable solutions and red points to unstable ones. White points correspond to highly unstable solutions, i.e., with a collision or the ejection of a planet during the 1 kyr of the simulation. The 3:2 resonances between Planet b and Planet c, and between Planet c and Planet d are highlighted.

References

Anglada-Escudé, G., Amado, P. J., Barnes, J., et al. 2016, *Nature*, 536, 437
 Astudillo-Defru, N., Delfosse, X., Bonfils, X., et al. 2017a, *A&A*, 600, A13
 Astudillo-Defru, N., Forveille, T., Bonfils, X., et al. 2017b, *A&A*, 602, A88
 Bonfils, X., Delfosse, X., Udry, S., et al. 2013, *A&A*, 549, A109
 Correia, A. C. M., Udry, S., Mayor, M., et al. 2005, *A&A*, 440, 751–758
 Cutri, R. M., Skrutskie, M. F., van Dyk, S., et al. 2003, *VizieR Online Data Catalog*, 2246, 0
 Dressing, C. D. & Charbonneau, D. 2015, *ApJ*, 807, 45
 Dumusque, X., Borsa, F., Damasso, M., et al. 2017, *A&A*, 598, A133
 Engle, S. G. & Guinan, E. F. 2011, in *Astronomical Society of the Pacific Conference Series*, Vol. 451, 9th Pacific Rim Conference on Stellar Astrophysics, ed. S. Qain, K. Leung, L. Zhu, & S. Kwok, 285
 Fabrycky, D. C., Lissauer, J. J., Ragozzine, D., et al. 2014, *ApJ*, 790, 146
 Faria, J. P., Haywood, R. D., Brewer, B. J., et al. 2016, *A&A*, 588, A31
 Foreman-Mackey, D., Hogg, D. W., Lang, D., & Goodman, J. 2013, *PASP*, 125, 306
 Fulton, B. J., Petigura, E. A., Howard, A. W., et al. 2017, *ArXiv e-prints*
 Gaidos, E. 2017, *MNRAS*, 470, L1
 Gillon, M., Triaud, A. H. M. J., Demory, B.-O., et al. 2017, *Nature*, 542, 456
 Goodman, J. & Weare, J. 2010, *Communications in applied mathematics and computational science*, 5, 65
 Grimm, S. L. & Stadel, J. G. 2014, *ApJ*, 796, 23
 Haywood, R. D., Collier Cameron, A., Queloz, D., et al. 2014, *MNRAS*, 443, 2517
 Laskar, J. 1990, *Icarus*, 88, 266–291
 Laskar, J. 1993, *Physica D Nonlinear Phenomena*, 67, 257–281
 Lo Curto, G., Pepe, F., Avila, G., et al. 2015, *The Messenger*, 162, 9
 Mann, A. W., Feiden, G. A., Gaidos, E., Boyajian, T., & von Braun, K. 2015, *ApJ*, 804, 64
 Mann, A. W., Feiden, G. A., Gaidos, E., Boyajian, T., & von Braun, K. 2016, *ApJ*, 819, 87
 Mayor, M., Lovis, C., & Santos, N. C. 2014, *Nature*, 513, 328
 Mayor, M., Pepe, F., Queloz, D., et al. 2003, *The Messenger*, 114, 20
 Muirhead, P. S., Johnson, J. A., Apps, K., et al. 2012, *ApJ*, 747, 144
 Pojmanski, G. 1997, *Acta Astron.*, 47, 467
 Rajpaul, V., Aigrain, S., Osborne, M. A., Reece, S., & Roberts, S. 2015, *MNRAS*, 452, 2269
 Rasmussen, C. E. & Williams, C. K. I. 2006, *Gaussian Processes for Machine Learning* (MIT, Press), 266
 Rein, H. & Liu, S.-F. 2012, *A&A*, 537, A128
 Rein, H. & Tamayo, D. 2015, *MNRAS*, 452, 376
 van Leeuwen, F. 2007, *A&A*, 474, 653
 Wright, D. J., Wittenmyer, R. A., Tinney, C. G., Bentley, J. S., & Zhao, J. 2016, *ApJ*, 817, L20
 Zechmeister, M. & Kürster, M. 2009, *A&A*, 496, 577

Appendix A: Gaussian process model

A quasi-periodic kernel was chosen to construct the elements of the covariance matrix of the observations. This type of covariance function was used in the past to model the effect of stellar active regions rotating in and out of view as the star revolves (Haywood et al. 2014; Rajpaul et al. 2015).

The elements of the covariance matrix are then given by $K_{ij} = K_{ij}^r + K_{ij}^w$, where

$$K_{ij}^r = k_{\{A; \tau; \mathcal{P}; \epsilon\}}(t_i, t_j) = A^2 \exp \left[-\frac{(t_i - t_j)^2}{2\tau^2} - \frac{2}{\epsilon} \sin^2 \left(\frac{\pi(t_i - t_j)}{\mathcal{P}} \right) \right]$$

represents the radial velocity effect related to the stellar rotational modulation, with $\{A, \tau, \mathcal{P}, \epsilon\}$ the hyperparameters associated with the covariance amplitude, the evolution timescale, the recurrence timescale (the rotational period of the star), and the smoothing parameter, respectively. The second term is a diagonal matrix with the quadratic sum of the internal velocity errors (σ_i) and an additional white noise component:

$$K_{ij}^w = (\sigma_i^2 + S_i \sigma_J^2 + S_i^+ \sigma_J^{+2}) \delta_{ij},$$

where S_i is an indicator variable which is one if observation i is taken before the HARPS fibre upgrade and zero otherwise, and viceversa for S_i^+ . δ_{ij} is the Kronecker delta function.

The prior distribution of the hyperparameters can be factorized in the marginal prior distributions described in Table B.2. Only the recurrence timescale \mathcal{P} was assigned an informative prior based on the analysis of the ASAS photometric measurements and the FWHM time-series.

Appendix B: Details on the MCMC analysis

The ensemble sampler of Goodman & Weare (2010) implemented in the emcee package (Foreman-Mackey et al. 2013) was used to sample the joint posterior distribution of the parameters and hyperparameters of the model. The prior assigned to the model parameters are listed in tables B.1 and B.2.

Initially, we chose to use 100 walkers on a 23-dimensional parameter space. The starting position of each walker was randomly drawn from the prior distribution. The burn-in period took approximately 500,000 steps, and the walkers were allowed to evolve still for around 100,000 steps. An issue usually encountered when running a MCMC algorithm is that some walkers get stuck in the local maxima, in this case related with period aliases and other features seen in the periodogram (Fig. 1). Because of this, we decided to retain only those walkers that explored the main periodogram peak for each planet. In this manner, 47 out of the 100 walkers were kept. The samples produced by these subset of walkers were used to initialise a second MCMC run using 300 walkers, which were run for 70,000 steps. This run had a mean acceptance fraction between walkers of around 25%. The characteristic autocorrelation length was between 3×10^2 and 1×10^3 steps. The average autocorrelation length over walkers was shorter than 1,000 steps for all parameters. We have then more than 700 independent samples per walker, which leads to a total of around 21,000 independent samples which are used for the parameter inference.

In Table B we list some characteristics of the posterior distribution based on the MCMC samples. Figure B.1 shows the 2-D marginal distributions of a selection of model parameters.

Table B.1. Prior distribution for the Keplerian curves and velocity offset between HARPS pre- and post-fibre upgrade. The priors are the same for each Keplerian, except for the period parameter. $\mathcal{U}(x_{min}, x_{max})$ is the uniform distribution between x_{min} and x_{max} .

Parameter & units	Prior distribution		
	YZ Cet b	YZ Cet c	YZ Cet c
P [days]	$\mathcal{U}(1.5, 2.5)$	$\mathcal{U}(2.5, 3.5)$	$\mathcal{U}(4.0, 5.2)$
K [m/s]	$\leftarrow \mathcal{U}(0, 10) \rightarrow$		
$\sqrt{\epsilon} \cdot \sin(\omega)$	$\leftarrow \mathcal{U}(-1, 1) \rightarrow$		
$\sqrt{\epsilon} \cdot \cos(\omega)$	$\leftarrow \mathcal{U}(-1, 1) \rightarrow$		
λ_0	$\leftarrow \mathcal{U}(0, 2\pi) \rightarrow$		
e	$\leftarrow \mathcal{U}(0, 1) \rightarrow$		
ΔV_{21} [m/s]			$\mathcal{U}(-10, 10)$

Table B.2. Prior distribution for the hyperparameters of the Gaussian Process kernel function. $\mathcal{J}(x_{min}, x_{max})$ is the Jeffreys distribution (log-flat), $\mathcal{U}(x_{min}, x_{max})$ is the uniform distribution between x_{min} and x_{max} .

Parameter	Prior distribution
A	$\mathcal{J}(10^{-4} \text{ m/s}, 10 \text{ m/s})$
τ	$\mathcal{J}(0.1 \text{ d}, 1000 \text{ d})$
\mathcal{P}	$N(83 \text{ d}, 15 \text{ d})$
ϵ	$\mathcal{U}(0.5, 1.5)$
σ_J	$\mathcal{U}(0 \text{ m/s}, 10 \text{ m/s})$
σ_J^+	$\mathcal{U}(0 \text{ m/s}, 10 \text{ m/s})$

Table B.3. Orbital elements using a model of three Keplerian plus a Gaussian Process. Values correspond to the maximum-a-posteriori (MAP) of the MCMC, with errors being the standard deviation of the MCMC samples. In the second line we report the 95% Highest-Density Interval (HDI).

N _{Meas}		211		
γ	[m/s]	28301.00 ± 0.30 [28300.37, 2831.62]	ΔV_{21}	[m/s] 0.01 ± 0.60 [-1.62, 0.85]
GP Hyperparametres				
σ_J	[m/s]	0.13 ± 0.28 [0.00, 0.95]	σ_J^+	[m/s] 0.64 ± 0.46 [0.00, 1.64]
$\log_{10}(A)$	[m/s]	0.14 ± 0.12 [-0.021, 0.348]	\mathcal{P}	[d] 79 ± 17 [51, 114]
$\log_{10}(\tau)$	[d]	0.68 ± 0.27 [0.28, 1.40]	ϵ	1.02 ± 0.29 [0.54, 1.50]
		YZ Cet b	YZ Cet c	YZ Cet d
P	[days]	1.96876 ± 0.00021 [1.96858, 1.96934]	3.06008 ± 0.00022 [3.05958, 3.06051]	4.65627 ± 0.00042 [4.65565, 4.65740]
K	[m/s]	1.48 ± 0.25 [0.92, 1.92]	1.68 ± 0.23 [1.22, 2.13]	1.72 ± 0.23 [1.13, 2.09]
e	[0..1[0.00 ± 0.12 [0.00, 0.41]	0.04 ± 0.11 [0.00, 0.37]	0.129 ± 0.096 [0.000, 0.311]
λ_0 at BJD _{ref} =2456845.73	[deg]	233.9 ± 9.4 [215.0, 254.2]	298.8 ± 8.3 [283.5, 316.4]	319.9 ± 8.8 [297.8, 333.4]
$\sqrt{e} \cdot \cos(\omega)$		0.02 ± 0.27 [-0.61, 0.43]	-0.19 ± 0.21 [-0.48, 0.32]	-0.06 ± 0.22 [-0.41, 0.43]
$\sqrt{e} \cdot \sin(\omega)$		-0.04 ± 0.26 [-0.47, 0.56]	-0.07 ± 0.24 [-0.63, 0.26]	0.36 ± 0.22 [-0.28, 0.55]
$M \sin i$	[M _{Earth}]	0.75 ± 0.13 [0.436, 0.964]	0.98 ± 0.14 [0.675, 1.267]	1.14 ± 0.17 [0.723, 1.389]
a	[au]	0.01557 ± 0.00052 [0.01444, 0.01661]	0.02090 ± 0.00070 [0.01938, 0.02229]	0.02764 ± 0.00093 [0.02564, 0.02948]
T_{eq} for $A_B=[0.75, 0]$	[K]	[347, 491]	[299, 423]	[260, 368]
BJD _{Trans} - 2456846.0	[days]	0.911 ± 0.095 [0.723, 1.137]	1.05 ± 0.14 [0.74, 1.35]	1.44 ± 0.16 [1.16, 1.79]
Trans. Prob.	[%]	5.7	4.1	2.9

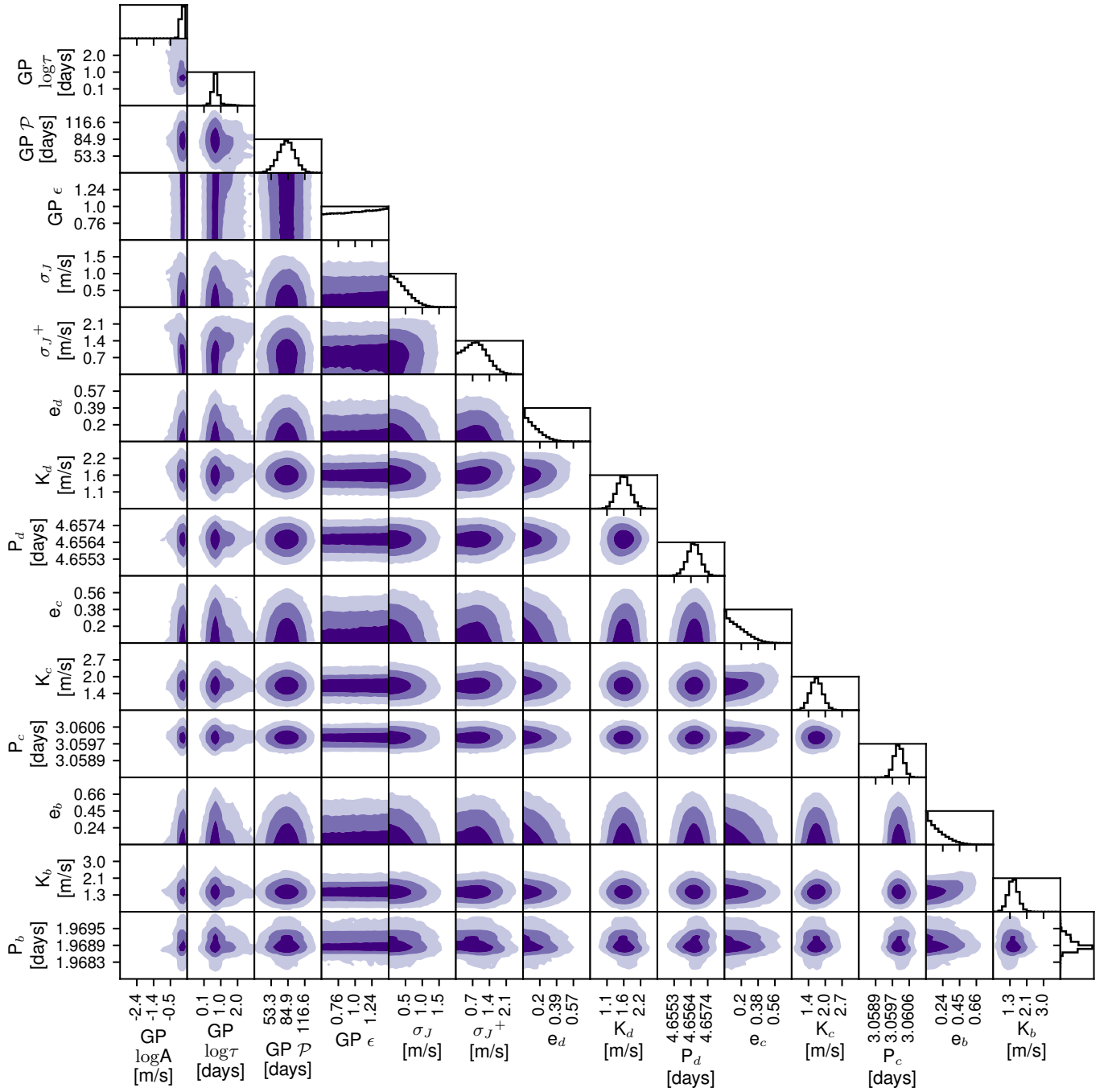


Fig. B.1. One- and two-dimensional marginal posterior distributions of selected model parameters. The contours represent the 68.27%, 95.45%, and 99.73% joint credible regions..